References

[1] Cookson, R. A., "An Analysis of Non-Constant Area Heat Addition Due to Combustion in a Supersonic Air-Steam," U.S. Air Force Office of Scientific Research Interim Scientific Report AFOSR-TR-75-1483, Sept. 1975.

[2] Pinckney, S. Z., "Integral Performance Predictions for Langley Scramjet Engine Module," NASA TM-X-74038, Jan. 1978.

[3] Ferri, A., Libby, P., and Zakkay, V., "Theoretical and Experimental Investigation of Supersonic Combustion," *Proceedings, 3rd Congress ICAS*, 1962, MacMillan Press, London, 1964, pp. 1089-1156.

[4] Hsia, H. T. S., "A Criteria for the Combustion Modes in Constant Area Combustors," ASME Paper 70-WA/AV-4, 1970.

[5] Henry, J. R. and Anderson, G. Y., "Design Considerations for the Airframe Integrated Scramjet," *Ist International Symposium on Air Breathing Engine*, Marseille, France, June 1972; also NASA TM-X-2895, 1973.

[6] Bussing, T. R. A. and Murman, E. M., "A One-Dimensional Unsteady Model of Dual Mode Scramjet Operation," AIAA Paper 83-0422, Jan. 1983.

[7] Billig, F. S. and Dugger, G. L., "The Interaction of Shock Waves and Heat Addition in the Design of Supersonic Combustors," *Twelfth Symposium (International) on Combustion*, The Combustion Institute, Pittsburgh, Pa., 1969, p. 1125.

[8] Waltrup, P. J. and Billig, F. S., "Prediction of Precombustion Wall Pressure Distributions in Scramjet Engines," *Journal of Spacecraft and Rockets*, Vol. 10, Sept. -Oct. 1973, pp. 620-622.

[9] Waltrup, P. J., Billig, F. S., and Stockbridge, R. D., "A Procedure for Optimizing the Design of Scramjet Engines," *Journal of Spacecraft and Rockets*, Vol. 16, May-June 1979, pp. 163-172.

[10] Waltrup, P. J., Dugger, G. L., Billig, F. S., and Orth, R. C., "Direct Connect Tests of Hydrogen-Fueled Supersonic Combustors," *Sixteenth Symposium (International) on Combustion*, The Combustion Institute, 1976, p. 1619.

[11] Anderson, G. Y., Eggers, J. M., Waltrup, P. J., and Orth, R. C., "Investigation of Step Fuel Injectors for an Integrated Modular Scramjet Engine," *CPIA Publication 281*, Vol. III, pp. 175-190.

[12] Waltrup, P. J., Billig, F. S., and Evans, M. C., "Critical Considerations in the Design of Supersonic Combustion Ramjet (scramjet) Engines," *Journal of Spacecraft and Rockets*, Vol. 18, July-Aug. 1981, pp. 350-356.

Heat Transfer in the Vicinity of a Large-Scale Obstruction in a Turbulent Boundary Layer

M. F. Blair*

United Technologies Research Center
East Hartford, Connecticut

Nomenclature

C_f = skin friction coefficient
H = boundary-layer shape factor, δ^*/θ
Re_θ = Reynolds number based on momentum thickness, $U_e\theta/\nu$
St = Stanton number, $h/\rho_e U_e c_p$
U_e = freestream velocity
X = distance from test section entrance
Y^+ = dimensionless distance from wall
δ = boundary-layer thickness
δ^* = boundary-layer displacement thickness
θ = boundary-layer momentum thickness

Presented as Paper 84-1723 at the AIAA 19th Thermophysics Conference, Snowmass, Colo., June 25-28, 1984; received Sept. 5, 1984. Revision received Nov. 1, 1984.

*Senior Research Engineer.

Introduction

HEAT transfer rates can be increased markedly in the region near a local obstruction in a boundary-layer flow, a manifestation of three-dimensional leading-edge horseshoe vortex effects. Examples of locations within gas turbine engines where leading-edge flow effects are known to cause increased heat transfer include the junction of airfoil leading edges with the platforms, the junction of support struts with the augmentor liner, and the region around dilution jet sites in combustors.

Leading-edge vortices develop just upstream ($\approx$1-4 obstruction widths) of an obstruction leading edge. The slower portion of the approaching boundary layer is unable to negotiate the local adverse streamwise pressure gradient and the boundary-layer fluid rolls up into a vortex oriented (at the plane of symmetry) parallel to the approach surface and perpendicular to the mainstream flow. This leading-edge vortex brings fluid with relatively high momentum nearer to the wall, increasing the velocity gradient normal to the wall and producing higher local skin friction. For flows with both velocity and temperature boundary layers, leading-edge effects produce higher local heat transfer both by increasing the local heat transfer coefficient and by transporting fluid at the freestream temperature closer to the surface.

Previous experimental work on three-dimensional flow effects near obstruction leading edges has been oriented to the study of aerodynamic effects.[1,2] An exception is the recent work by Han et al.,[3] which investigated horseshoe vortex effects on the heat transfer distribution on a cylindrical obstruction. In constrast to Ref. 3, which focused on changes to the heat transfer distribution over the obstruction surface, the present study was designed to examine the effects of a horseshoe vortex on the heat transfer to the surface beneath the approach boundary layer. The present study was designed to provide both flowfield and surface heat transfer distribution data for a fixed geometry and set of experimental test conditions.

Description of Test Equipment

This study was conducted in a low-speed, open-circuit, low-turbulence wind tunnel with a straight test section 50-cm wide, 20-cm high and 2.3-m long. The test surface along which the approach boundary layer developed consisted of the 50-cm-wide horizontal lower wall of the test section. Rods 6 mm^2 located on the top and bottom surfaces at the test section entrance tripped and artifically thickened the boundary layer.

A forward-facing rectangular block, spanning the test section from top to bottom, was mounted along the centerline 0.9 m from the test section entrance. The block was 15.2 cm wide, 90 cm long, and had a circular arc trailing edge to reduce unsteadiness in the wake. The lower wall of the test section, along with the approach boundary layer developed, was a uniform heat flux surface. This test surface consisted of a block of rigid urethane foam covered with thin (0.025 mm) stainless steel foil. Regulated d.c. current passing through the foil provided a nearly uniform surface heat flux. Local Stanton numbers were determined by measuring the local surface temperature reached with the uniform heat flux boundary condition. This particular heat transfer model fabrication technique is designed to permit measurement of local heat transfer coefficients since conduction both along the thin foil and through the rigid foam substrate is negligible.

The temperature distribution and therefore the Stanton number distribution over the uniform heat flux plate was determined using an AGA Model 780 color display scanning

infrared (IR) camera. The scanning camera viewed the test surface from above through an IR "window" of vinylidene chloride-vinyl chloride copolymer.

Velocity profile data for the boundary layer developing along the test surface were obtained with miniature pitot probes. Flow visualization patterns on the horizontal surface were obtained using the ink/oil of wintergreen techniques of Langston and Boyle.[4]

Additional information concerning the wind tunnel characteristics, the heat transfer surface, and the IR techniques are given in the text and reference list of Ref. 5.

Test Conditions

All experimental testing for this study was conducted with a velocity at the test section entrance of 9.1 m/s. For this tunnel speed the static pressure in the test section was approximately 2-cm H_2O above ambient barometer. The freestream temperature was 31°C. Velocity profile data for the approach boundary layer were obtained along the tunnel centerline at $x=63$ and 90 cm (the model leading-edge location) from the test section entrance. Both sets of profile data were obtained with the rectangular obstruction removed. The profile station at $x=63$ cm, however, was sufficiently far upstream to be independent of the presence of the obstruction. Table 1 lists the measured boundary-layer dimensions and properties.

Both profiles, when plotted in universal coordinates, exhibited logarithmic behavior from $50<Y^+<600$. This result, combined with the shape factors given in Table 1, indicates that the approach boundary layer was fully turbulent. The skin friction coefficients C_f for the present profiles were determined from a least-squares fit of the velocity profile data to the law-of-the-wall. Comparison of the present data with the equilibrium turbulent correlation of Coles[6] indicates that the present skin friction coefficients were approximately 10% too high for equivalent momentum thickness Reynolds numbers. This result indicates that the boundary-layer profiles still showed slight nonequilibrium effects at the model leading edge, probably a result of the coarse upstream trip. From the perspective of a velocity power law, both profiles could be well represented by a 1/7 power shape.

The above boundary-layer profile data were obtained for adiabatic flow, i.e., there was no power supplied to the surface foil. Approach boundary-layer test conditions were also evaluated for the case of uniform wall heat flux. Stanton numbers determined from thermocouples mounted upstream of the model, both on and to either side of the tunnel centerline, indicate that the approach flow was two-dimensional and that the upstream heat transfer distribution was in good agreement with standard correlations for two-dimensional, fully turbulent boundary-layer flow.

Results

The surface-streamline pattern established around the upstream end of the rectangular obstruction is presented in Fig. 1. The streakline pattern clearly shows a region of local backflow upstream of the model face and local separation bubbles on both model sides downstream of the corners. A

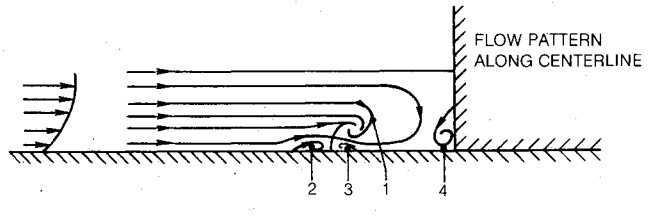

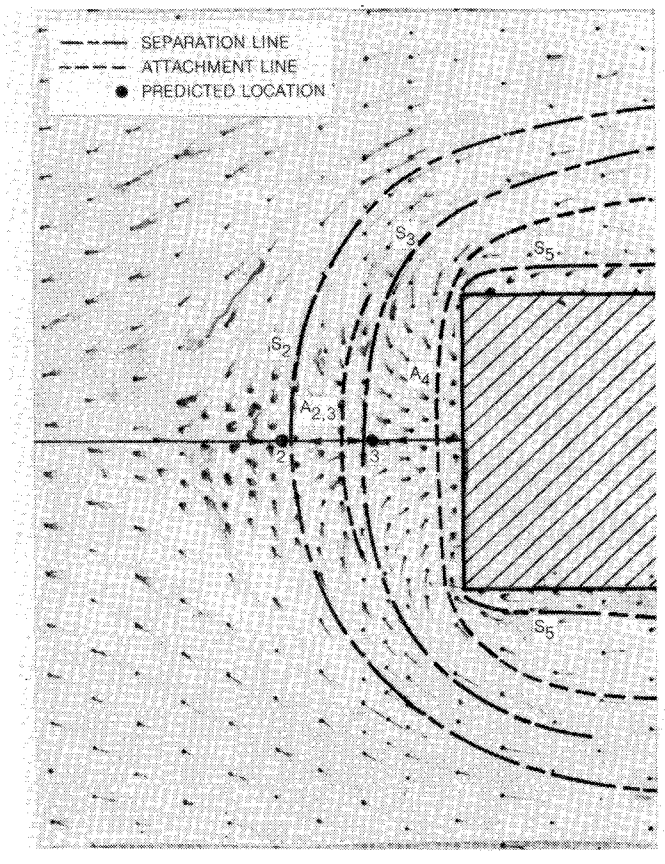

Fig. 1 Flow visualization pattern on plane horizontal tunnel wall.

Table 1 Boundary-layer characteristics

x, cm	δ, cm	δ^*, cm	θ, cm	H	Re_θ	C_f
63	3.71	0.445	0.334	1.333	1863	0.00415
90	3.84	0.498	0.372	1.343	2055	0.00393

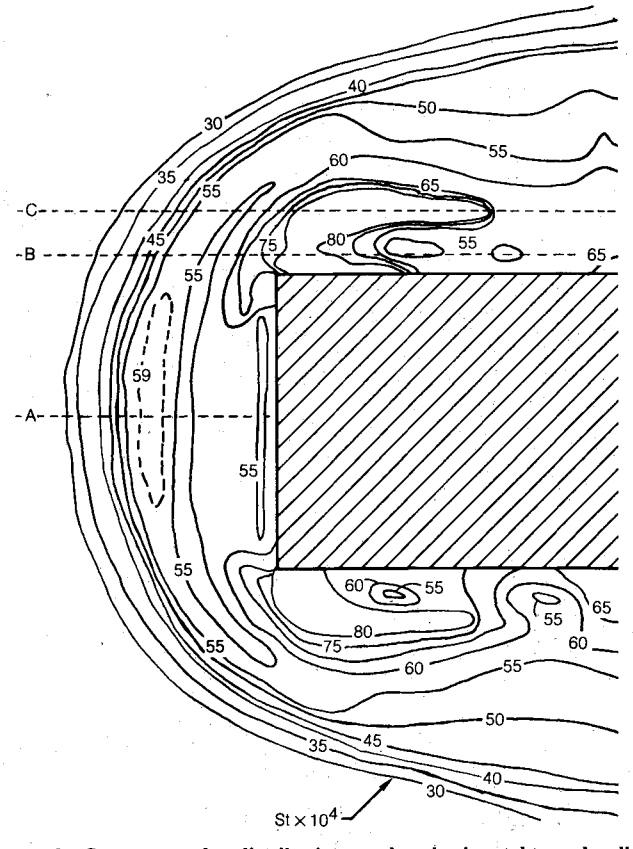

Fig. 2 Stanton number distribution on plane horizontal tunnel wall.

pattern of such complexity leaves considerable room for speculation concerning the three-dimensional flow pattern. One intepretation of the streaklines, following the examples and reasoning of Hunt et al.[1] and Baker,[2] proposes a system of four vortices upstream of the obstruction. This four vortex system is sketched in Fig. 1 and includes the main horseshoe vortex (1), a pair of counterrotating vortices (2 and 3) beneath the main vortex, and a small vortex (4) tucked in the model face-surface corner. For this flow pattern lines S_2 and S_3 delineate the loci of three-dimensional separation of vortices 2 and 3 from the surface. Line $A_{2,3}$ represents the attachment line between vortices 2 and 3.

As can be seen from an examination of Fig. 1, evidence to support existence of vortices 2 and 3 is meager. An alternative interpretation of the flow visualization pattern could be that only vortices 1 and 4 exist and that the location of the upstream separation line was unsteady. In this interpretation lines S_2 and S_3 mark the boundaries of motion of the unsteady separation.

Whatever the physical significance of lines S_2 and S_3, it is interesting to note that their locations are in excellent agreement with a similar pair of lines observed by Baker[2] upstream of a circular cylinder. Using the correlations of Ref. 2 and replacing the cylinder diameter with the obstruction width, the centerline locations of S_2 and S_3 were computed. These predicted locations are shown as dots 2 and 3 in Fig. 1 and show excellent agreement with the present results. Also shown in Fig. 1 are estimates of the locations of the attachment line for vortex 4 and the lines of separation (5) associated with the sidewall separation bubbles. A sample demonstration numerical prediction of this flow (computed with a three-dimensional Navier-Stokes procedure) is given in Ref. 5.

Contours of constant Stanton number determined from the IR thermograms are presented in Fig. 2. The absolute accuracy of the Stanton number values is estimated to be $\pm 5\%$. The two most striking features of Fig. 2 are the complexity of the heat transfer pattern established by the presence of the obstruction and the magnitude of the effects on the local heat transfer. Along the centerline (locus A, Fig. 2) the peak Stanton number was almost 100% higher than the undisturbed two-dimensional value. The peak Stanton number (along loci B and C, Fig. 2) was 160% greater than the undisturbed level.

Conclusions

1) Flow visualization patterns recorded in the leading-edge region of the rectangular obstruction revealed a complex three-dimensional flow pattern. The locations of a pair of separation lines upstream of the obstruction were well predicted using the correlations of Baker.[2]

2) Heat transfer distribution measurements on the plane surface revealed that the obstruction established a complex heat transfer pattern. Stanton numbers as much as 100% greater than the undisturbed two-dimensional level were recorded upstream of the obstruction along the tunnel centerline.

References

[1] Hunt, J. C., Bell, C. J., Peterka, J. A. and Wood, H., "Kinematical Studies of the Flows Around Free or Surface Mounted Obstacles; Applying Topology to Flow Visualization," *Journal of Fluid Mechanics,* Vol. 86, Pt. 1, 1978, pp. 197-200.

[2] Baker, C. J., "The Turbulent Horseshoe Vortex," *Journal of Wind Engineering and Industrial Aerodynamics,* Vol. 6, 1980, pp. 9-23.

[3] Han, L. C., Ma, C., and Rapp, J. R., "The Endwall Influence in Heat Transfer From a Single Cylinder (The Horseshoe Vortex Effect)," Paper 83-TOKYO-11GTC-3, TOKYO International Gas Turbine Conference, 1983.

[4] Langston, L. S. and Boyle, M. T., "A New Surface-Streamline Flow-Visualization Technique," *Journal of Fluid Mechanics,* Vol. 125, 1982, pp. 53-57.

[5] Blair, M. F., "Heat Transfer in the Vicinity of a Large-Scale Obstruction in a Turbulent Boundary Layer," AIAA Paper 84-1723, June 1984.

[6] Coles, D. E., "The Turbulent Boundary Layer in a Compressible Fluid," Rand Rept. R-403-PR, 1962.